Science of the Total Environment 970 (2025) 178968

Contents lists available at ScienceDirect

Science of the Total Environment

journal homepage: www.elsevier.com/locate/scitotenv

Representing particulate nitrate photolysis over seawater improves CMAQ ozone predictions over the contiguous United States

Golam Sarwar [a,*], Fahim Sidi [a], Heather Simon [b], Barron H. Henderson [a], Jeff Willison [a], Rob Gilliam [a], Christian Hogrefe [a], Kristen Foley [a], Rohit Mathur [a], Wyat Appel [a]

[a] Center for Environmental Measurement & Modeling, U.S. Environmental Protection Agency, Research Triangle Park, NC 27711, USA
[b] Office of Air Quality Planning and Standards, U.S. Environmental Protection Agency, Research Triangle Park, NC 27711, USA

HIGHLIGHTS

- Photolysis of particulate nitrate over seawater enhances ozone over the U.S.
- The pathway produces more ozone over the western than over the eastern U.S.
- The pathway improves model spring-time ozone underestimation
- The pathway improves model summer-time ozone underestimation over the western U.S.
- Boundary condition effect contributes 68 % of particulate nitrate photolysis in the U.S.

GRAPHICAL ABSTRACT

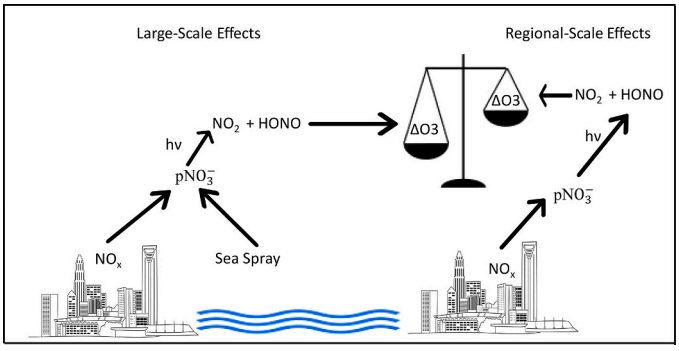

ARTICLE INFO

Editor: Hai Guo

Keywords:
Photolysis
Particulate nitrate
Ozone
Model performance
Air quality
CMAQ

ABSTRACT

We implement particulate nitrate (pNO_3^-) photolysis into the Community Multiscale Air Quality (CMAQv5.5) model and examine the impact of pNO_3^- photolysis on air quality over the contiguous U.S. using 12-km horizontal grids for May–September 2018. Model results show that pNO_3^- photolysis increases ozone in each month compared to simulations without the pNO_3^- photolysis and increases monthly mean of 24-h surface ozone over the modeling domain by 9.3 ppb (32 %) in May, 8.0 ppb (29 %) in June, 5.6 ppb (20 %) in July, 5.1 ppbv (17 %) in August and 3.6 ppbv (13 %) in September. These increases are larger over the western U.S. than over the eastern U.S. and improve the negative ozone bias over the western U.S. Over the eastern U.S., incorporating pNO_3^- photolysis improves the underestimation of ozone in May but slightly deteriorates the positive ozone bias in June–September. However, the deterioration of the ozone bias occurs only at the lower end of observed ozone. Incorporating the effect improves the bias at the higher end of observed ozone and improves the comparison of model diurnal ozone with observed data over the western U.S. but deteriorates it over the eastern U.S. Model sensitivity results suggest that boundary condition effect of pNO_3^- photolysis contributes 68 % and pNO_3^- photolysis within the limited area domain contributes 32 % of the total impact of pNO_3^- photolysis on ozone over the U.S. in May.

* Corresponding author at: US EPA, 109 T.W. Alexander Drive, Research Triangle Park, NC 27711, USA.
E-mail address: sarwar.golam@epa.gov (G. Sarwar).

https://doi.org/10.1016/j.scitotenv.2025.178968
Received 11 January 2025; Received in revised form 22 February 2025; Accepted 22 February 2025
Available online 4 March 2025
0048-9697/Published by Elsevier B.V.

1. Introduction

Tropospheric ozone (O_3) is a harmful air pollutant with detrimental impacts on human health and ecosystems (US EPA, 2020a). Ozone mixing ratios have decreased substantially in the United States (U.S.) over the past two decades (Simon et al., 2015; Lefohn et al., 2017; Gaudel et al., 2018; Wells et al., 2021) but there remain numerous areas that are still in nonattainment for U.S. O_3 National Ambient Air Quality Standards (NAAQS) of 70 ppb (https://www.epa.gov/green-book/green-book-8-hour-ozone-2015-area-information). O_3 levels in the U.S. result from a combination of local and regional formation from U.S. anthropogenic emissions, natural sources, and long-range transport of anthropogenically formed O_3 from upwind regions outside of the U.S. The U.S. EPA reports that the relative importance of these sources varies by time of year and location (US EPA, 2020b). Modeling simulations indicate that O_3 originating from sources other than U.S. anthropogenic emissions (i.e., natural + international) is in the range of about 30 ppb averaged across all days and locations but is highest in the spring, at high elevation locations in the western U.S. due to transport from the free troposphere and in near-border areas where short-range transport from large urban areas along the border is important (US EPA, 2020b). The importance of long-range transport of anthropogenic O_3 from upwind regions outside of the U.S. is most important during spring months and in high-elevation western U.S. locations. These findings are based on analyses using comprehensive chemistry-transport models which are well suited for determining O_3 source contributions. However, uncertainty in model estimates stem from uncertainty in inputs (e.g., emissions) as well as uncertainty in the underlying model representation of atmospheric physical and chemical processes (Russel and Dennis, 2000; Dennis et al., 2010; Napelenok et al., 2011). Recent experimental and observational studies (Ye et al., 2016; Ye et al., 2017; Reed et al., 2017; Romer et al., 2018; Shi et al., 2021; Zhu et al., 2022; Anderson et al., 2023) suggest that nitrate photolysis in aerosol particles is accelerated several orders of magnitude relative to the bulk solution reaction and have identified particulate nitrate (pNO_3^-) photolysis as one important chemical uncertainty. pNO_3^- had previously been treated as a sink for reactive nitrogen in most models, but pNO_3^- is now believed to be a reservoir from which reactive nitrogen can be recycled through photolysis. Photolysis of pNO_3^- has the potential to increase the lifetime of oxides of nitrogen (NO_y) and is thus critically important to accurately represent the contribution of long-range international transport to O_3 levels in the U.S. In previous work, we simulated the impacts of including this chemistry on modeled O_3 mixing ratios by using coarse-resolution (108-km) hemispheric CMAQ (Mathur et al., 2017) model simulations (Sarwar et al., 2024). Here, we further explore the importance of this chemistry by pairing the hemispheric model simulations with finer-resolution 12-km model simulations over the contiguous U.S. to better characterize the impact of large scale forcings on regional and local-scale O_3 formation.

2. Methodology

The Community Multiscale Air Quality (CMAQ) model (www.epa.gov/cmaq) is a state of the science air quality model containing comprehensive treatment of all important atmospheric processes and has been used in many air quality research studies and regulatory activities in and outside the U.S. It contains detailed treatment of emissions, advection and diffusion, gas-phase chemistry, aerosol processes, deposition, and cloud processes. The CMAQ model is periodically updated and released to the public. CMAQv5.5 was released in October 2024 (www.epa.gov/cmaq; doi: https://doi.org/10.5281/zenodo.13883210) and has been used in this study. The modeling domain for this study covers the entire contiguous U.S., Canada, and Mexico and is discretized using 12-km horizontal grids and 35 vertical layers of varying thickness with a model top reaching to 50 hpa and a first layer height of approximately 20-m.

Meteorological fields for driving the CMAQ model were prepared using the Weather Research and Forecasting model version 4.3.3 (WRFv4.3.3; Skamarock et al., 2021). WRF has been used for retrospective meteorological simulations at the U.S. EPA for many years (Appel et al., 2017; U.S. EPA, 2019; Gilliam et al., 2021). The physics options followed the standard US EPA configuration. Key physics parameterizations include the RRTMG shortwave and longwave radiation schemes (Iacono et al., 2008) and the Kain-Fritsch 2 (KF2, Kain, 2004) convective parameterization scheme with the subgrid cloud feedback to the radiation (Alapaty et al., 2012; Herwehe et al., 2014) option. The Morrison double-moment microphysics (Morrison et al., 2009) has been used for many years in WRF. The P-X Land Surface model (LSM) (Pleim and Xiu, 1995), the Asymmetric Convective Model, version 2 (ACM2) Planetary Boundary Layer (PBL) (Pleim, 2007), and Pleim surface layer schemes (Pleim, 2006) were used to resolve surface-atmospheric interactions where the National Land Cover Dataset with 40 land use categories (NLCD40) defined the surface characteristics.

Four-Dimensional Data Assimilation (FDDA) in the form of grid nudging was used for winds, temperature and moisture above the planetary boundary layer. FDDA has been found to significantly reduce the uncertainty of atmospheric state variables in the free troposphere (Stauffer and Seaman, 1990) and is a key model setting for retrospective meteorology inputs for air quality modeling (Gilliam et al., 2021). Three-hourly National Center for Environmental Prediction (NCEP), North American Model (NAM)-based 12 km analyses were the source of FDDA inputs. The P-X LSM used indirect soil moisture and temperature nudging (Pleim and Gilliam, 2009) that requires NAM-based 2-m temperature and moisture from the same NCEP NAM analysis. The obsgrid re-analysis tool was used for both FDDA and P-X soil nudging fields to further improve the analysis inputs that has been shown to further reduce modeling error (Gilliam et al., 2021).

WRF predictions were evaluated against observed surface and upper-air meteorology as well as precipitation and shortwave radiation over the U.S. Root Mean Square Error (RMSE) of model predicted temperature, water vapor mixing ratio, wind speed, and wind direction are calculated using observed data over the U.S. (Table S.1). The WRF simulation had expected levels of error. Monthly error in temperature was <2.1 K, water vapor mixing ratio was <1.7 g kg^{-1}, 10-m wind speed was <1.7 m s^{-1}, and wind direction was 31–33 degrees. All of these follow published benchmarks like US EPA (2019) and other historical US EPA modeling. Thus, WRF predicted meteorological field is deemed suitable for driving the CMAQ model.

Model-ready emissions were generated using the Sparse Matrix Operator Kernel Emissions (SMOKE). Anthropogenic emissions were obtained from the 2017 National Emissions Inventory (USEPA, 2021) and were adjusted for year 2018 using year-specific data for sources when available (e.g., onroad, nonroad, oil and gas, power plants, volatile chemical products) or scaling factors following the methodology in Foley et al. (2023). Biogenic emissions were generated using in-line Biogenic Emission Inventory System (Bash et al., 2016) as implemented in CMAQv5.5 (doi: https://doi.org/10.5281/zenodo.13883210; https://github.com/USEPA/CMAQ/wiki/CMAQ-Release-Notes:Emissions-Updates:-BEIS-Biogenic-Emissions). Lightning NO_x (NO_x = NO + NO_2) emissions were calculated in-line (Kang et al., 2019). Procedures used in estimating fire emissions for the US EPA Air Quality Time Series project (EQUATES) (Beidler et al., 2024) are used. Sea-spray emissions in CMAQ (Gantt et al., 2015) are speciated into several aerosol species by mass (gm/g) (Millero, 1996): Cl^-, Na^+, SO_4^{2-}, Ca^{2+}, Mg^{2+}, K^+, and Br^-. We include an additional tracer species for sea-salt in CMAQ as it does not separately track sea-salt concentration and use its molar concentration to calculate enhancement factor.

Chemical mechanisms used in air quality models typically do not include the photolysis of pNO_3^-. Nitric acid (HNO_3) photolysis frequency is well known, and most air quality models employ HNO_3 photolysis. However, several recent studies suggest that pNO_3^- can undergo

photolysis in the atmosphere. pNO_3^- photolysis frequency is usually expressed with an enhancement factor (EF) that is simply a ratio of pNO_3^- photolysis frequency and HNO_3 photolysis frequency. Several studies (Romer et al., 2018; Shi et al., 2021) suggest that EF is small (1−30). In contrast, other studies (Ye et al., 2016; Ye et al., 2017; Reed et al., 2017; Zhu et al., 2022; Anderson et al., 2023) suggest EF is much higher and can reach several hundreds. Anderson et al. (2023) recently completed a field campaign and suggest that EF is not constant but varies with many factors e.g., temperature, relative humidity, pH, particle composition and particle aging, presence of dust and other factors. They suggest EF is generally high at low pNO_3^- concentration and low at high pNO_3^- concentration.

Ye et al. (2016) proposed that pNO_3^- photolysis produces HONO (nitrous acid) and NO_2 (nitrogen dioxide) as follows:

$$pNO_3^- \xrightarrow{h\nu} 0.67 \times HONO + 0.33 \times NO_2 \quad (1)$$

Dang et al. (2023) and Shah et al. (2023) implemented pNO_3^- photolysis in GEOS-Chem using the following parametrization for EF:

$$EF = 100 \times max\left(\frac{[SSA]}{[SSA] + [pNO_3^-]}, 0.1\right) \quad (2)$$

Where [SSA] is the molar concentration of sea-salt and [pNO_3] is the molar concentration of pNO_3. Sarwar et al. (2024) implemented eqs. 1 and 2 into CMAQv5.4 and quantified the impact of the chemistry on O_3 over the Northern Hemisphere. Here, we also use the same chemistry and EF but apply this chemistry using simulations with finer 12-km grid resolution over the contiguous U.S. using an updated version of CMAQ (www.epa.gov/cmaq; doi: https://doi.org/10.5281/zenodo.13883210).

Two different CMAQ simulations were completed for the study. The first simulation was completed using the Carbon Bond 6, release 5 (CB6r5) chemical mechanism (Yarwood et al., 2020) without any pNO_3 photolysis chemistry. Boundary and initial conditions for this simulation were generated from the hemispheric CMAQ results without any pNO_3 photolysis. The second simulation was completed using the CB6r5 with the pNO_3 photolysis reaction described in eq. 1 and the EF parameterization from eq. 2. Boundary conditions for the second simulation were generated from the hemispheric CMAQ results with pNO_3 photolysis (Sarwar et al., 2024). Boundary conditions for the second simulation contained lower pNO_3 concentrations and higher NO_2, HONO, and O_3 mixing ratios compared to those used for the first simulation. Differences in model results of the second and first simulations are attributed to the pNO_3 photolysis. Both simulations started on April 20, 2018, and ended on September 30, 2018. The first 11 days are used as model spin-up period and the results for May–September are analyzed. May is taken as a representative month for spring while September is taken as a representative month for fall. The months of June, July, August comprised the summer season. To examine impacts of the pNO_3 photolysis without including the effect of pNO_3 photolysis in the boundary conditions, we completed an additional sensitivity simulation for May. The sensitivity simulation included pNO_3 photolysis but utilized boundary conditions from the hemispheric model without the pNO_3 photolysis. The details of each simulation performed for this study are presented in Table 1.

Table 1
Simulation cases.

Case	Chemical mechanism	Boundary and initial condition	Simulation period	Comments
A	CB6r5 without any pNO_3^- photolysis	Hemispheric CMAQ results without any pNO_3^- photolysis	May to September	B-A = Combined impacts of pNO_3^- photolysis occurring over the model domain and integrating the effect of pNO_3^- photolysis into boundary condition B-C = Impacts of integrating the effect of pNO_3^- photolysis into boundary condition C-A = Impacts of pNO_3^- photolysis occurring over the model domain
B	CB6r5 with pNO_3^- photolysis	Hemispheric CMAQ results with pNO_3^- photolysis	May to September	
C	CB6r5 with pNO_3^- photolysis	Hemispheric CMAQ results without any pNO_3^- photolysis	May	

3. Results

3.1. Impact on pNO_3^-

We focus on daytime (solar radiation absorbed on ground >5-watt m^{-2}) model predictions since the pNO_3 photolysis is active only during the day. Model predicted May – September daytime surface layer mean pNO_3 concentrations and the impacts of the pNO_3 photolysis on pNO_3 are shown in Fig. 1(a) and (b), respectively. The model without pNO_3 photolysis predicts pNO_3 concentrations >0.25 μg m^{-3} over portion of California and the surrounding coastal water, the mid-west, portions of western Canada, and portion of seawater. pNO_3 concentrations are predicted to be <0.25 μg m^{-3} over other areas. pNO_3 photolysis reduces pNO_3 concentrations by 0.02–0.2 μg m^{-3} over seawater, parts of California, and the mid-west but increases pNO_3 concentrations by <0.05 μg m^{-3} over some isolated areas. The locations of the greatest decreases in pNO_3 due to photolysis generally coincide with locations with the largest pNO_3 concentrations in the model simulation except for Alberta, Canada where pNO_3 photolysis had little impact on pNO_3 concentrations despite relatively high concentrations. The reduction of pNO_3 occurs primarily due to the direct loss of pNO_3 from photolysis and lower pNO_3 transported into the modeled domain through the boundary conditions. pNO_3 concentrations in Alberta are very high resulting in a very low EF which in turn generated only small impact on pNO_3 concentrations.

Monthly Mean Bias (MB; calculated as observed concentrations – modeled concentrations) of model predicted pNO_3 concentrations without and with the pNO_3 photolysis is shown in Fig. 1(c) and (d) for the western and eastern U.S., respectively (see Fig. S.1 for definition of the western and eastern U.S.). Over the western U.S., the model without pNO_3 photolysis (red bars in Fig. 1(c)) reproduces observed data in May as MB is close to zero. Model pNO_3 concentrations without the pNO_3 photolysis are lower than the observed concentrations in other months as MB is negative in each month. The model with pNO_3 photolysis (blue bars in Figs. 1(c)) marginally affects the pNO_3 concentrations as MBs are close to those obtained with the pNO_3 photolysis. Over the eastern U.S., model pNO_3 concentrations without the pNO_3 photolysis are consistently lower than the observed data as MB is negative in each month. Again, the model treatment with pNO_3 photolysis only marginally affects the pNO_3 concentrations and MBs are very similar to those obtained in the model simulations without pNO_3 photolysis.

3.2. Impact on NO_2

Model predicted mean daytime NO_2 mixing ratios without the pNO_3 photolysis and the changes due to the inclusion of pNO_3 photolysis are shown in Fig. 2a and b, respectively. The model without pNO_3 photolysis produces NO_2 mixing ratios >800 pptv over many urban areas which have relatively large NO_2 emissions. It predicts relatively lower levels of NO_2 away from large NO_2 emissions sources over rural areas and seawater. Elevated NO_2 mixing ratios along the shipping tracks are also evident in comparison to surrounding marine locations in Fig. 2(a). pNO_3 photolysis enhances NO_2 levels over seawater, large areas of the western U.S., Mexico, and Canada and reduces NO_2 levels over large

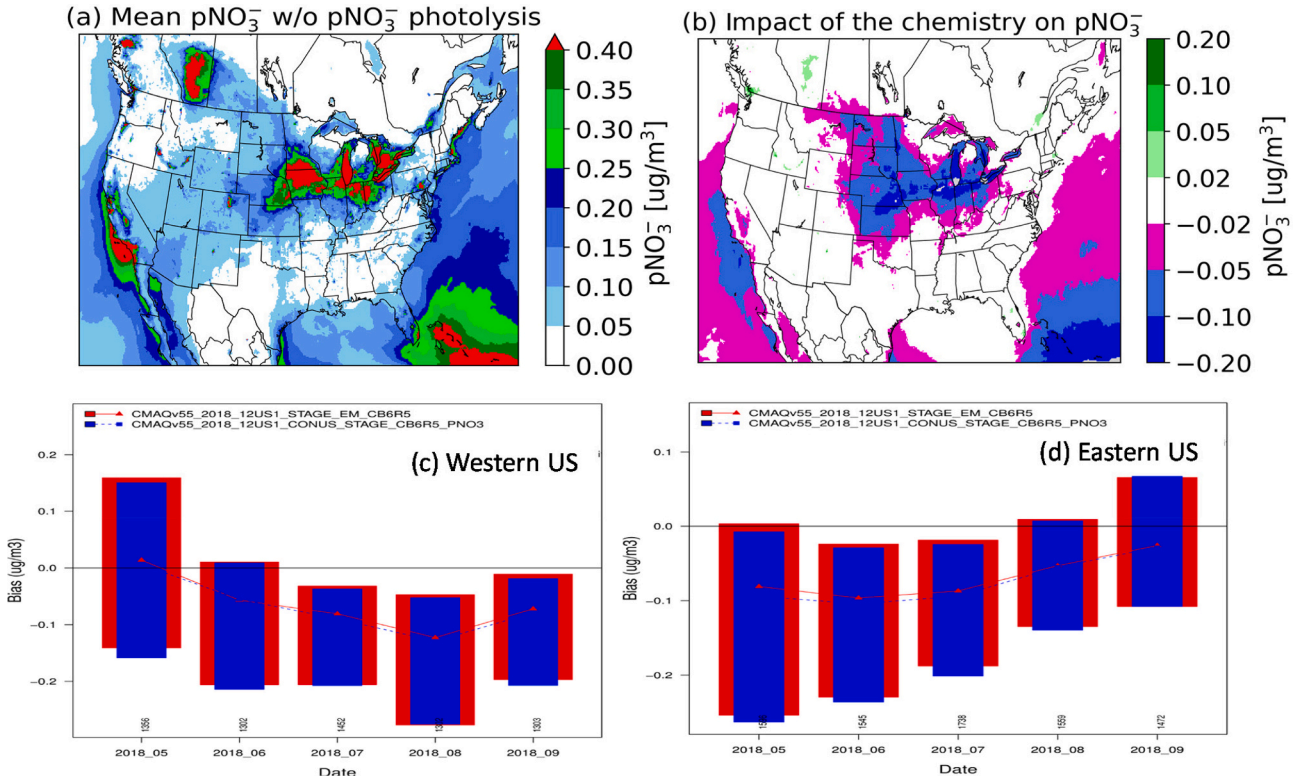

Fig. 1. (a) May – September daytime mean pNO_3^- concentrations without pNO_3^- photolysis (Case A) (b) impact of pNO_3^- photolysis on daytime May–September mean pNO_3^- concentrations (Case B – Case A) (c) monthly Mean Bias (MB) of pNO_3^- concentrations without (red) and with (blue) the pNO_3^- photolysis over the western U.S. and (d) Monthly MB of pNO_3^- concentrations without (red) and with (blue) the pNO_3^- photolysis over the eastern U.S. Weekly (all hours) data from the Clean Air Status and Trends Network (CASTNET) and 24-h average data from Chemical Speciation Network (CSN) and Interagency Monitoring of Protected Visual Environments (IMPROVE) are combined for comparison with modeled data. Red color represents model without pNO_3^- photolysis and blue color represents model with pNO_3^- photolysis. The number of model/observation pairs for each month is shown above the x-axis in (c) and (d).

areas of eastern U.S. Higher impacts are predicted over water than over land. NO_2 enhancements occur primarily due to the production of NO_2 via the pNO_3 photolysis and the contribution from the boundary condition. Over the eastern U.S., NO_2 mixing ratios in the model without the pNO_3 photolysis are relatively high compared to the western U.S. As shown in Fig. 3, pNO_3 photolysis enhances O_3 regionally. Reactions of NO_2 with additional O_3 and NO_2 with NO_3 (gas-phase nitrate radical) reduce night-time NO_2 causing the morning levels to be lower than the corresponding values of the model without the pNO_3 photolysis. In the eastern U.S., the lower morning NO_2 level causes lower daytime NO_2 despite production from the pNO_3 photolysis while in the western U.S. the increased production along with transport from the boundaries outweigh the chemical loss due to increased O_3 mixing ratios. The reaction of NO_2 with additional hydroxyl radical also contributes to the lower daytime NO_2 in the eastern U.S. in the simulation with pNO_3 photolysis compared to the simulation without pNO_3 photolysis. Model predictions are compared to data (all hours) from Air Quality System (AQS) over the western and eastern U.S. in Fig. 2(c) and 2(d). The AQS sites are generally located in urban areas with higher NO_2 mixing ratios. Monthly MB without the pNO_3 photolysis is negative in each month which indicates that model predictions are lower than the observed data. The model with pNO_3 photolysis, however, does not change MB in the western or eastern U.S. Model changes near the surface are small; consequently, there are no changes in MB. Model predicted NO_x mixing ratios are compared to data (all hours) from AQS over the western and eastern U.S. in Fig. 2(e) and 2(f). Consistent with the NO_2 results, the model with pNO_3 photolysis, however, does not change MB of NO_x mixing ratios in the western or eastern U.S.

We compare CMAQ NO_2 tropospheric vertical column densities (VCD) with retrievals from the Ozone Monitoring Instrument (OMI; Krotkov et al., 2017) and describe mean bias without and with pNO_3 photolysis in Fig. S.2(a) and S.2(b), respectively. CMAQ-OMI bias calculations use all OMI retrievals over the domain for May to September after excluding retrievals based on quality flags or effective cloud fraction >0.3. OMI pixels are regridded to CMAQ's lambert conformal grid using an area-weighted average approach as implemented in CMAQ Satellite Processor (https://github.com/barronh/cmaqsatproc v0.4.1) resulting in 70,089 valid grid cell pairs per day on average (51 % of possible cells) for comparison. To compare to CMAQ, the OMI retrieved slant path column density (SCD) is converted to a VCD (=SCD/($\Sigma w_z S_{zs}$)) using the reported scattering weights (w_z: increasing with altitude) and simulation dependent NO_2 shape factor ($S_{zs} = VCD_{zs}/VCD_s$). The shape factor weighted w_z scales the SCD to account for both viewing geometry and retrieval sensitivity (Krotkov et al., 2017). Using CMAQ for the shape factor ensures consistent resolution and vertical distribution within the bias calculation. The OMI VCD will be smaller (larger) when the CMAQ simulation has more (less) NO_2 aloft because w_z increases with altitude. Biases obtained without pNO_3 photolysis are negative with a mean value of $-0.50 \pm 0.37 \times 10^{15}$ molecules cm^{-2} and a Normalized Mean Bias (NMB) of -45 ± 16 %, where values are mean $\pm$ std. over all pixels in the domain. The model with pNO_3 photolysis generally produces positive bias with a mean value of $0.10 \pm 0.20 \times 10^{15}$ molecules cm^{-2} and a NMB of 23 ± 34 %. The change in bias can be broken down into two distinct components: (1) a direct change in the predicted NO_2 column and (2) a change to the OMI VCD. First, pNO_3 photolysis produces NO_2 and increases model average vertical column density by $0.36 \pm 0.07 \times 10^{15}$ molecules cm^{-2} (81 $\pm$ 38 %). Second, pNO_3 photolysis decreases the processed OMI vertical columns by changing the derived air mass factor. pNO_3 photolysis disproportionately increases the partial columns (VCD_{zs}) aloft where satellite

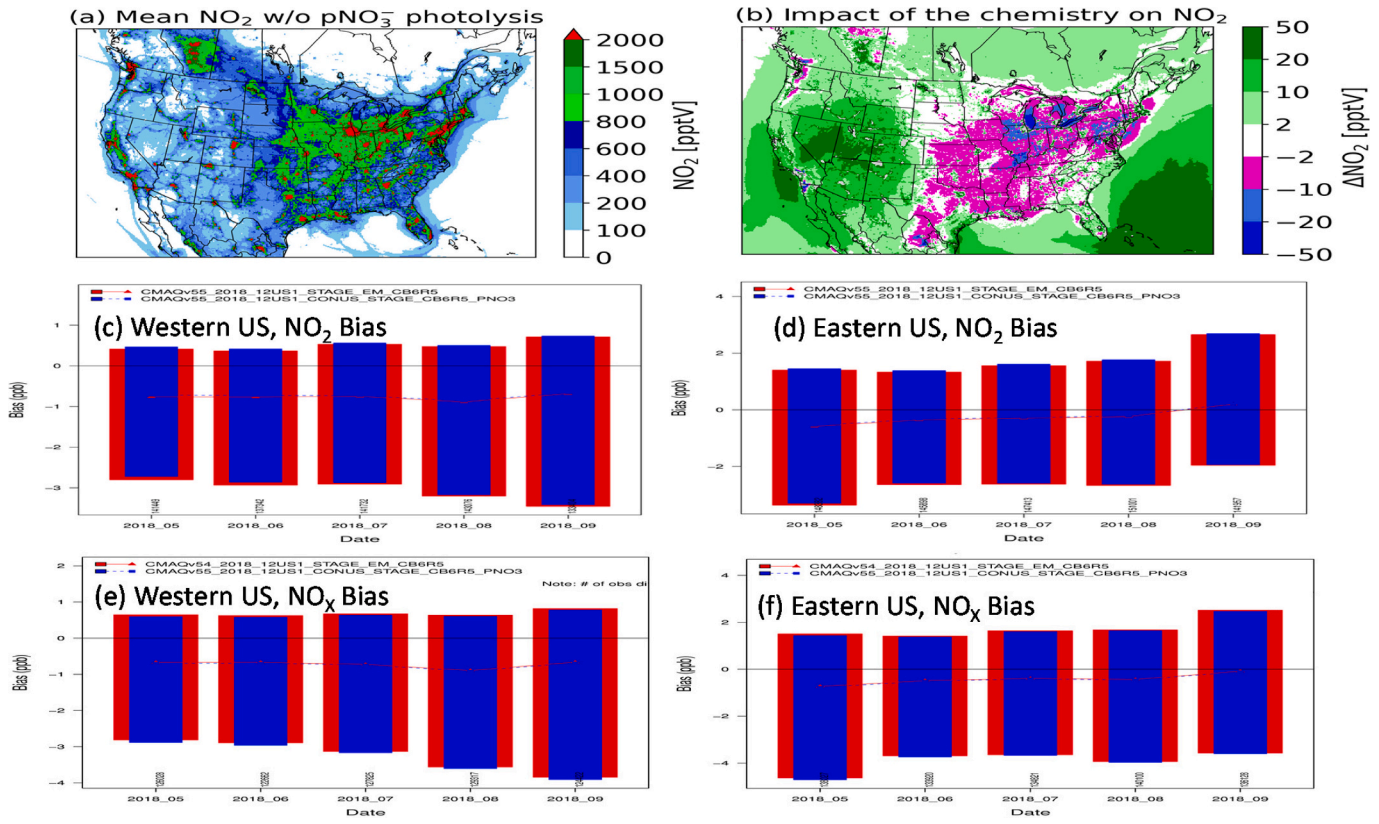

Fig. 2. (a) May–September daytime mean NO_2 mixing ratios without pNO_3^- photolysis (Case A) (b) impact of pNO_3^- photolysis on NO_2 mixing ratios (Case B - Case A) (c) Monthly MB of NO_2 mixing ratios (all hours) without and with the pNO_3^- photolysis over the western U.S. at AQS sites (d) Monthly MB of NO_2 mixing ratios (all hours) without and with the pNO_3^- photolysis over the eastern U.S. at AQS sites. (e) Monthly MB of NO_x mixing ratios (all hours) without and with the pNO_3^- photolysis over the western U.S. at AQS sites (f) Monthly MB of NO_x mixing ratios (all hours) without and with the pNO_3^- photolysis over the eastern U.S. at AQS sites. Red color represents model without pNO_3^- photolysis and blue color represents model with pNO_3^- photolysis. The number of model/observation pairs for each month is shown above the x-axis in (c) and (d).

sensitivity (w_z) is high and, therefore, decreases the OMI VCD by $-0.26 \pm 0.23 \times 10^{15}$ molecules cm^{-2} (-21 ± 11 %). The direct addition of NO_2 in the column and the change in the shape factor both substantially contribute to the net change in estimated bias.

3.3. Impact on HONO

Model predicted May – September daytime mean HONO mixing ratios without the pNO_3 photolysis and the changes with the HONO photolysis are shown in Fig. S.3a and Fig. S.3b, respectively. Model HONO production depends on NO_2 (Sarwar et al., 2008). Relatively higher HONO levels are predicted over many urban areas due to elevated NO_2 levels over those areas. Lower values are predicted over rural areas and seawater. Higher values along the shipping track are also noticeable. pNO_3 photolysis enhances HONO mixing ratios over seawater and some land areas. However, its impact over land is generally small due to lower EF. Higher impacts are seen over seawater than over land. Reduction of HONO occurs over some land areas due to lower NO_2 levels. Impact of pNO_3 photolysis on HONO over land is generally small where other HONO production pathways are important. To evaluate the impact of the chemistry on HONO, observed HONO data are needed in remote areas. Model predictions are not compared to any observed data since such data are not available in remote areas within the modeling domain.

We previously compared model prediction with observed HONO data from a remote area off the west coast of Africa (Sarwar et al., 2024) (which is located outside the modeling domain used in this study) and model predictions with the pNO_3 photolysis compared much better with observed data.

3.4. Impact on O_3

Unlike daytime results reported for other pollutants which included hours where solar radiation absorbed on ground is >5-watt m^{-2}, daytime O_3 is calculated as the daily maximum 8-h (MDA8) O_3 mixing ratio, which is also the regulatory metric in the U.S. Mean MDA8 O_3 mixing ratios without the pNO_3 photolysis are shown in Fig. 3(a). Higher values are predicted over land than over seawater. pNO_3 photolysis enhances mean MDA O_3 mixing ratios by 3.0–17.0 ppbv over the U.S. and larger enhancements occur over the western U.S. than over the eastern U.S. (Fig. 3(b)). The largest enhancement occurs in May. These results are consistent to those presented in Sarwar et al. (2024).

Monthly MDA8 O_3 MB was calculated by using model predicted O_3 and observed data from the AQS (Fig. 3(c-d)) and CASTNET (Fig. 3(e-f)) sites over the western and eastern U.S. Over the western U.S., the model without pNO_3 photolysis underpredicts observed data (negative MB) at the AQS sites. The extent of the negative bias is largest in May and then the bias improves in each month but the model still underpredicts the observed data in each month. The model with pNO_3 photolysis eliminates almost all negative biases and produces slightly positive mean biases in each month. Over the eastern U.S., the model without pNO_3 photolysis produces mixed bias compared to the observed data at AQS sites, with a negative mean bias in May, nearly zero mean bias in June and July, and positive mean bias in August and September. The model with the pNO_3 photolysis eliminates the negative MB in May but produces positive bias in June–September. A similar trend is also noticeable over the western and eastern U.S. at the CASTNET sites (Fig. 3(e-f)). Thus, over the western U.S, the model without the pNO_3 photolysis underpredicts monthly mean MDA8 O_3 throughout the May–September

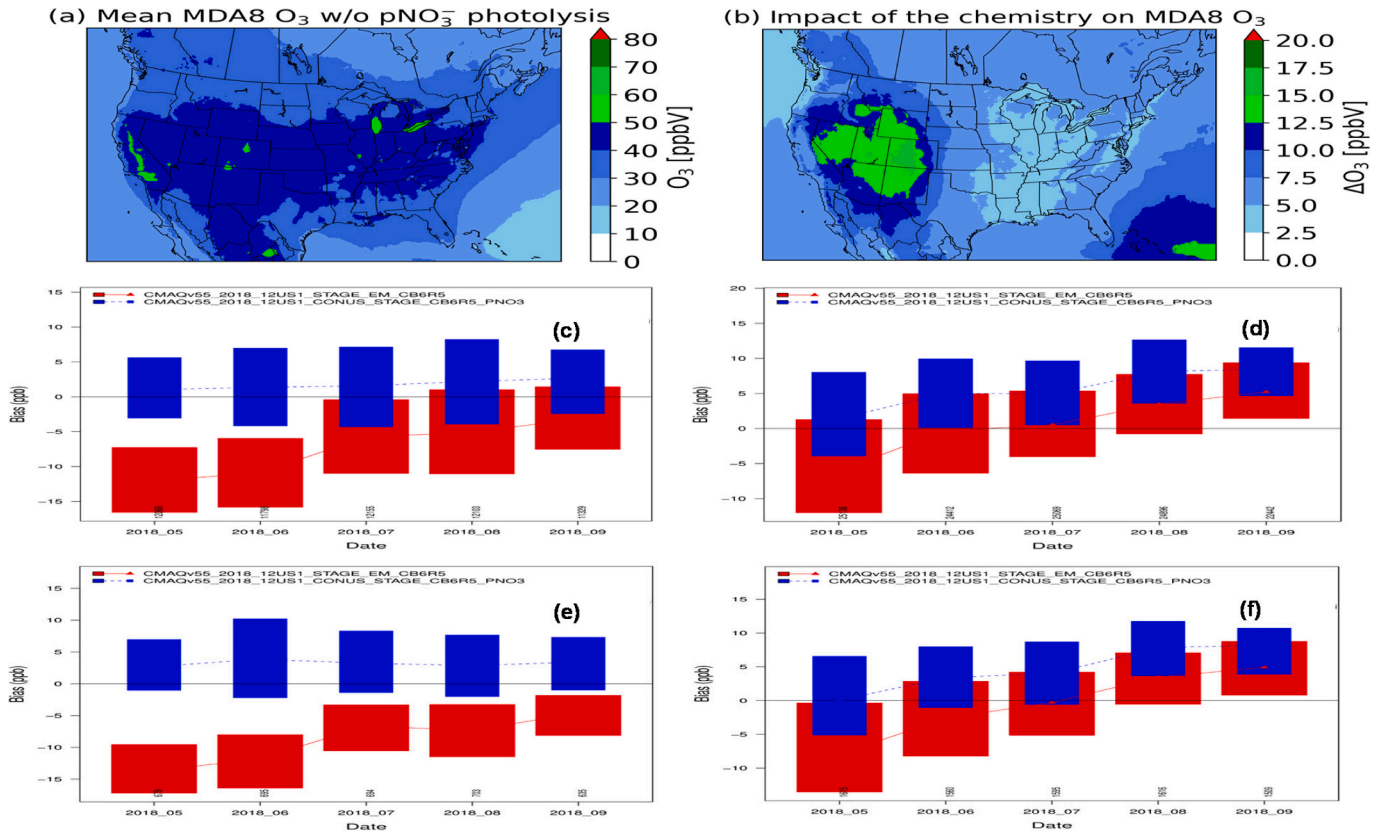

Fig. 3. (a) May – September mean MDA O_3 mixing ratios in simulation without pNO_3^- photolysis (Case A) (b) impact of pNO_3^- photolysis on mean MDA O_3 mixing ratios (Case B - Case A) (c) Monthly MB of MDA8 O_3 mixing ratios without (red) and with (blue) the pNO_3^- photolysis over the western U.S. at AQS sites (d) Monthly MB of MDA8 O_3 mixing ratios without (red) and with (blue) the pNO_3^- photolysis over the eastern U.S. at AQS sites (e) Monthly MB of MDA8 O_3 mixing ratios without (red) and with (blue) the pNO_3^- photolysis over the western U.S. at CASTNET sites (f) Monthly MB of MDA8 O_3 mixing ratios without (red) and with (blue) the pNO_3^- photolysis over the eastern U.S. at CASTNET sites. The number of model/observation pairs for each month is shown above the x-axis in (c-f).

period analyzed in this study and the pNO_3 photolysis substantially improves the model under-predictions. Over the eastern U.S., the model without the pNO_3 photolysis underpredicts monthly mean MDA8 O_3 in May but produces nearly zero MB or over-predicts in June–September and the pNO_3 photolysis improves the model under-predictions in May but results in positive bias in the remaining months.

Spatial plots of monthly mean MDA8 O_3 MB in May at AQS sites are shown in Fig. 4(a-b). The model without pNO_3 photolysis substantially under-predicts MDA8 O_3 producing large negative bias over the U.S. The magnitude of the under-predictions is larger over the western U.S. than over the eastern U.S. pNO_3 photolysis increases MDA8 O_3 mixing ratios and substantially improves the bias over the U.S. eliminating the negative mean bias over large areas of the U.S. and producing slightly positive mean bias. However, negative bias is still persistent in some areas of the U.S. (western U.S., northeast, and the mid-west). Thus, pNO_3 photolysis substantially improves the modeled May O_3 under-prediction that has been reported in previous studies (Appel et al., 2021). Spatial plots of monthly mean MB in July at AQS sites are shown in Fig. S.4(a-b). The model without pNO_3 photolysis under-predicts MDA8 O_3 (negative bias) over the western U.S. but produces positive bias over the eastern U.S. pNO_3 photolysis improves model MDA8 O_3 under-prediction over the western U.S. but further exacerbates over-predictions of O_3 over the eastern U.S.

Building upon the monthly mean results shown in Figs. 3(c)–3(f), daily time series of MB were calculated over the eastern and western U. S. by using model predicted MDA8 O_3 and observed data from the AQS sites in each region. Over the eastern U.S., the model without pNO_3 photolysis produces mixed bias (Fig. 5(a)). The base model simulation without pNO_3 photolysis produces negative MDA8 O_3 bias for many days in May and June, mixed bias for remaining days in May–June and July, and positive bias in August and September. The model with the pNO_3 photolysis improves the negative bias on many days in May and June but over-predicts on other days. Over the western U.S., the model without pNO_3 photolysis produces negative bias (Fig. 5(b)). The magnitude of the negative bias is the largest in May and then the negative bias improves but persists in subsequent months. The model with pNO_3 photolysis eliminates the negative bias on most days. Time series of daily MDA8 O_3 MB at the CASTNET sites over the western and eastern U.S. are shown in Fig. S.5(a-b). Similar to the results at the AQS sites, the model without pNO_3 photolysis produces negative bias over the western U.S. and the pNO_3 photolysis improves the negative bias on all days over the western U.S. but only improves the bias in May and part of June and deteriorates it on other days over the eastern U.S. Thus, the model without pNO_3 photolysis produces mixed bias over the eastern U. S. and the pNO_3 photolysis improves the negative bias in May for all days but tends to deteriorate the bias in June–September. The Model without pNO_3 photolysis produces negative daily bias over the western U.S. and the pNO_3 photolysis improves the negative bias for almost all days in May–September modeled period.

We show MB of MDA8 O_3 at the AQS sites as a function of observed MDA8 mixing ratio bins in Fig. 6(a, c) by combining all data during the simulation. Over the eastern U.S., the model without pNO_3 photolysis produces positive bias when observed MDA8 O_3 is below 50 ppbv and negative bias when observed MDA8 O_3 is above 50 ppbv (Fig. 6(a)). The pNO_3 photolysis further deteriorates the bias on observed days below 50 ppbv but improves the bias on observed days above 50 ppbv. Over the western U.S., the model without pNO_3 photolysis produces positive bias on days with observed MDA8 O_3 below 30 ppbv and negative bias on

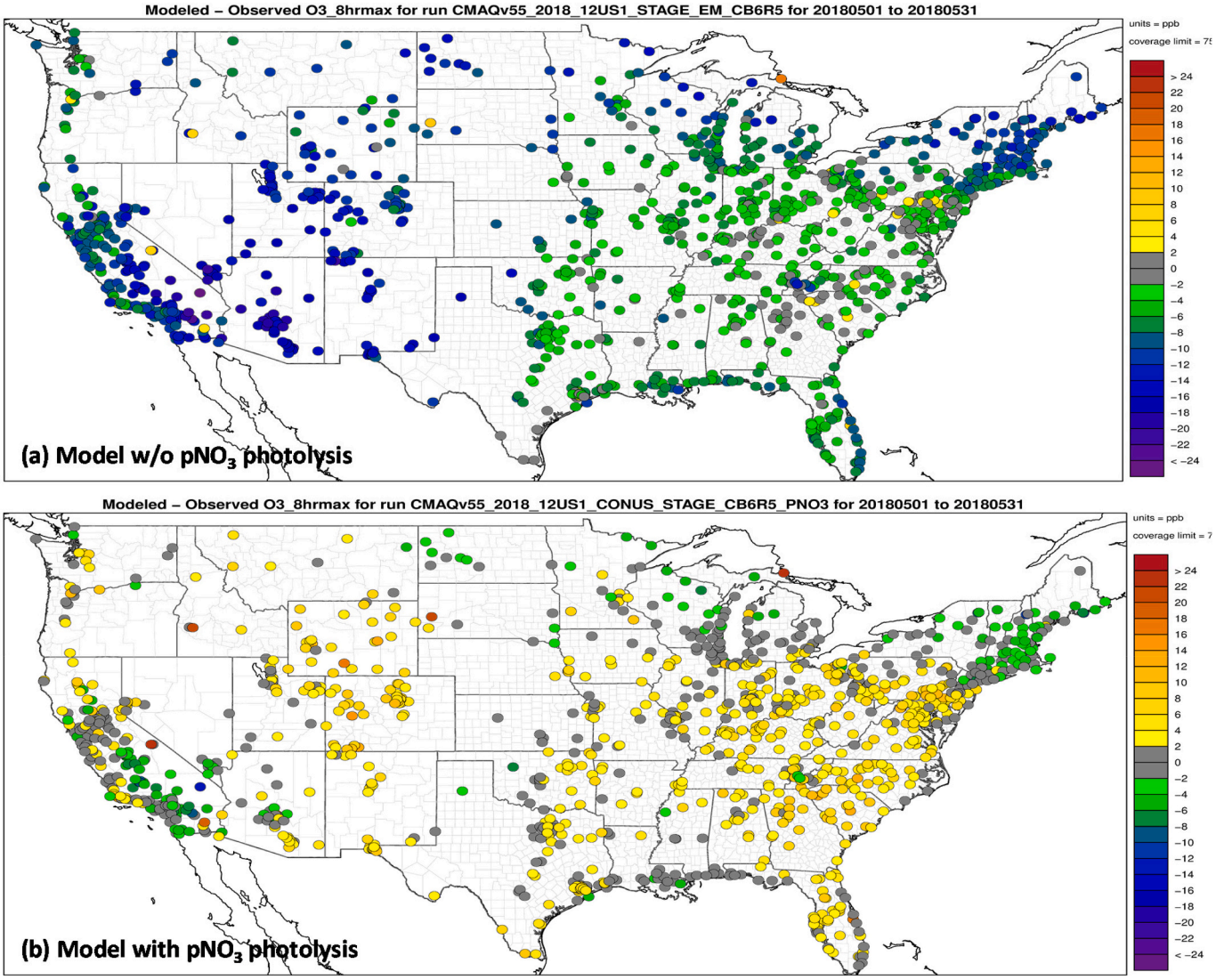

Fig. 4. (a) Spatial plot of May MB of MDA8 O_3 without the pNO_3^- photolysis at the AQS sites (b) Spatial plot of May MB of MDA8 O_3 with the pNO_3^- photolysis at the AQS sites.

days with observed MDA8 O_3 above 30 ppbv (Fig. 6(c)). The pNO_3 photolysis further deteriorates the bias on observed days below 30 ppbv but improves the bias on observed days above 30 ppbv. Root Mean Square Error (RMSE) of MDA8 O_3 as a function of observed data are shown in Fig. 6(b, d). The pNO_3 photolysis increases the error at the lower ranges of observed data but reduces the error at the higher end of observed data. MB and RMSE of MDA8 O_3 at the CASTNET sites as a function of observed data are shown in Fig. S.6(a-d). Results at the CASTNET sites are consistent to those shown in Fig. 6(a-d) at the AQS sites.

We compare model diurnal patterns of hourly O_3 with observed data for two representative months: May and July. The model predicted median diurnal pattern of O_3 in May are compared to the observed data at the CASTNET and AQS sites in Fig. 7(a-d). Observed O_3 mixing ratios are lower at night and higher during the day peaking in the mid-afternoon. Both model simulations reproduce the diurnal pattern of observed data. However, the model without pNO_3 photolysis substantially (>10 ppbv) under-predicts the observed data both at night and during the day in the western U.S. The pNO_3 photolysis enhances O_3 mixing ratios and substantially improves the comparison with observed data. Over the eastern U.S., the model without pNO_3 photolysis also under-predicts the observed data and the pNO_3 photolysis enhances O_3 mixing ratios and improves the comparison with observed data but tends to over-estimate observed data for some hours. The model predicted median diurnal pattern of O_3 in July are compared to the observed data at the CASTNET and AQS sites in Fig. S.7(a-d). pNO_3 photolysis improves the comparison with observed data in the western U.S. However, it results in overprediction in the eastern U.S.

Ozonesonde data from the National Oceanic and Atmospheric Administration's Earth System Research Laboratory are available at three sites (Trinidad Head, California; Boulder, Colorado and Huntsville, Alabama) in the U.S. (Johnson, et al., 2018). Modeled O_3 mixing ratios are compared to observed data at Trinidad Head, California in Fig. 8. Model results without pNO_3 photolysis are generally lower than observed data in May–August and the model results with pNO_3 photolysis agree better with observed data at all altitudes. In September, the comparison produces mixed performance. Model results with pNO_3 photolysis agree better with observed data at 1–3 km while model results without pNO_3 photolysis agree better with observed data at other altitudes. Model O_3 mixing ratios are compared with observed data at Boulder, Colorado and Huntsville, Alabama in Fig. S.8. In Boulder, model results without pNO_3 photolysis are consistently lower than observed data in May and June, and model results with pNO_3 photolysis agree better with observed data at all altitudes. In July–August, model

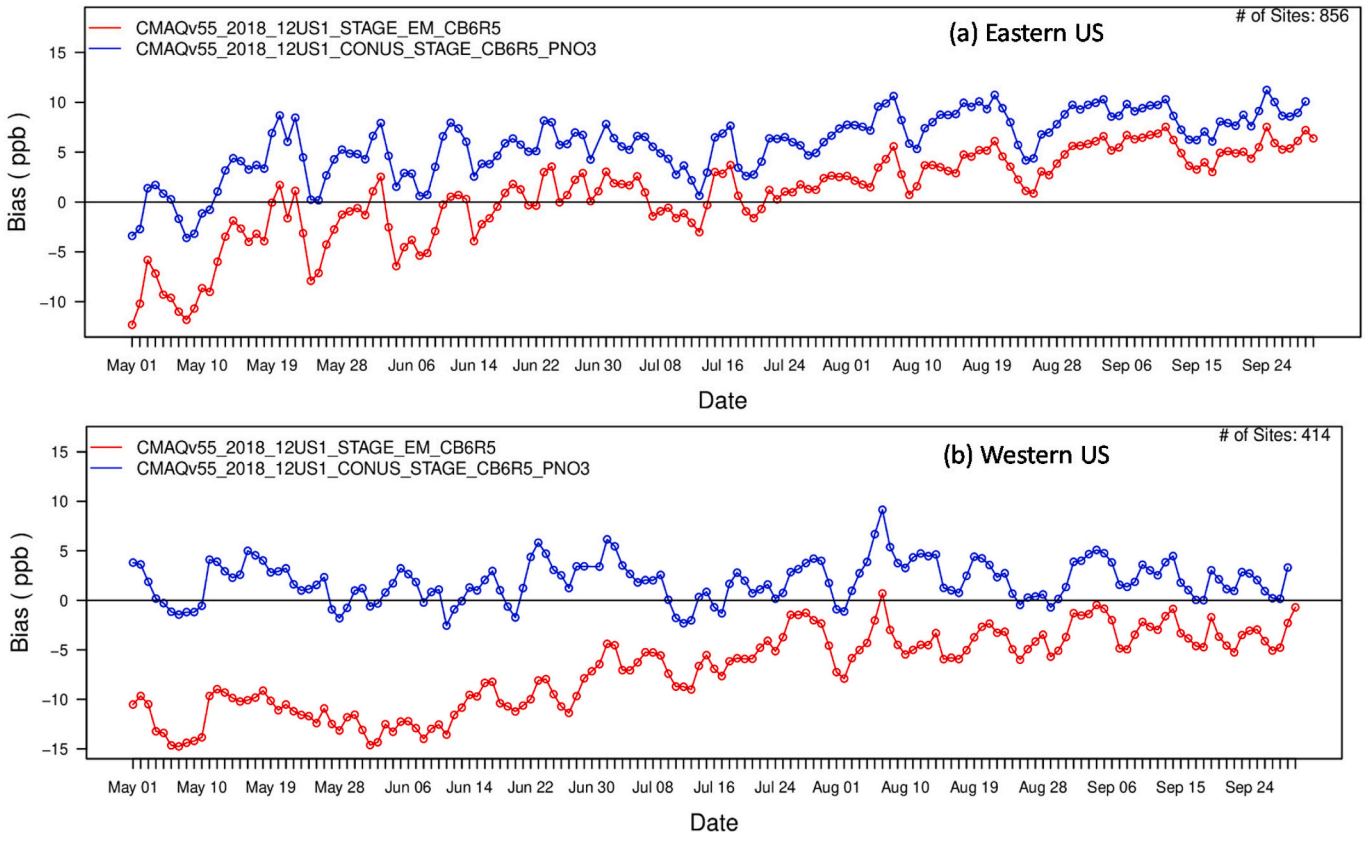

Fig. 5. (a) Daily bias of MDA8 hour O_3 without and with the pNO_3^- photolysis over the eastern U.S. at AQS sites (b) Daily bias of MDA8 hour O_3 without and with the pNO_3^- photolysis over the western U.S. at AQS sites. Red color represents model without pNO_3^- photolysis and blue color represents model with pNO_3^- photolysis.

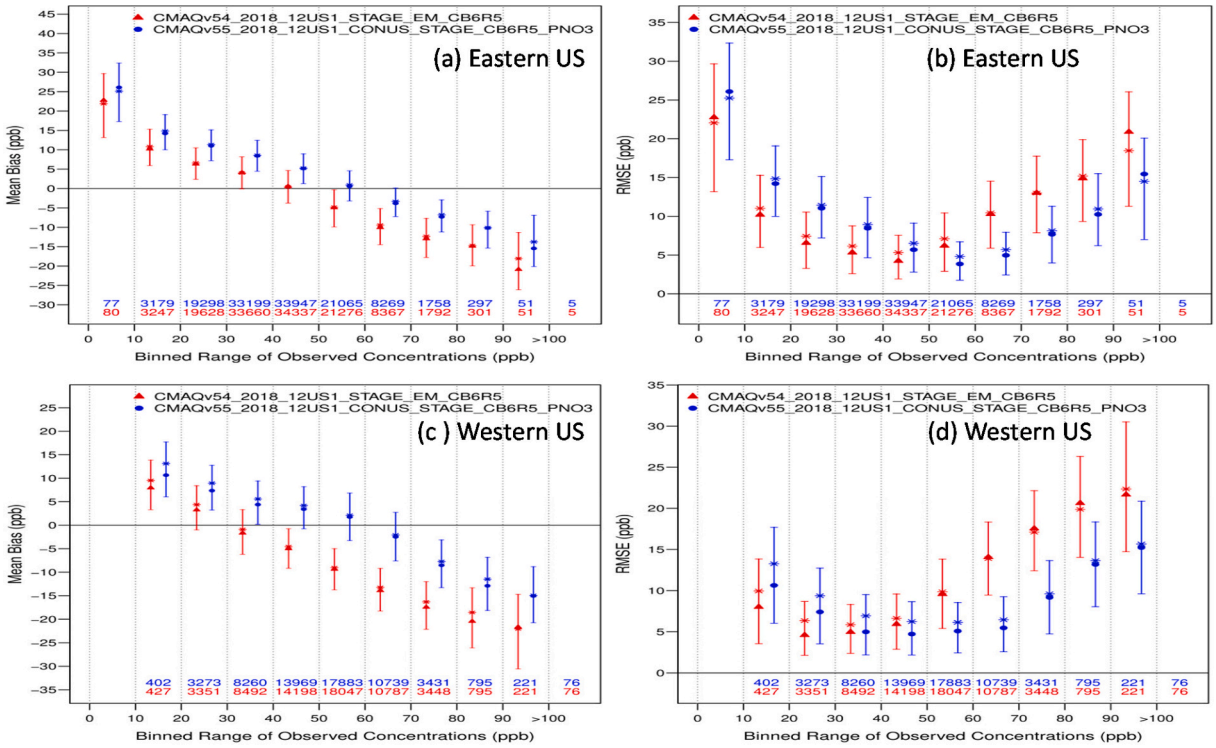

Fig. 6. MB of MDA8 O_3 without and with the pNO_3^- photolysis at AQS sites as a function of observed data: (a) the eastern U.S. (c) the western U.S. RMSE of MDA8 O_3 without and with the pNO_3^- photolysis at AQS sites as a function of observed data: (b) the eastern U.S. (d) the western U.S. The number of model/observation pairs for each bin is shown above the x-axis. Red color represents model without pNO_3^- photolysis and blue color represents model with pNO_3^- photolysis.

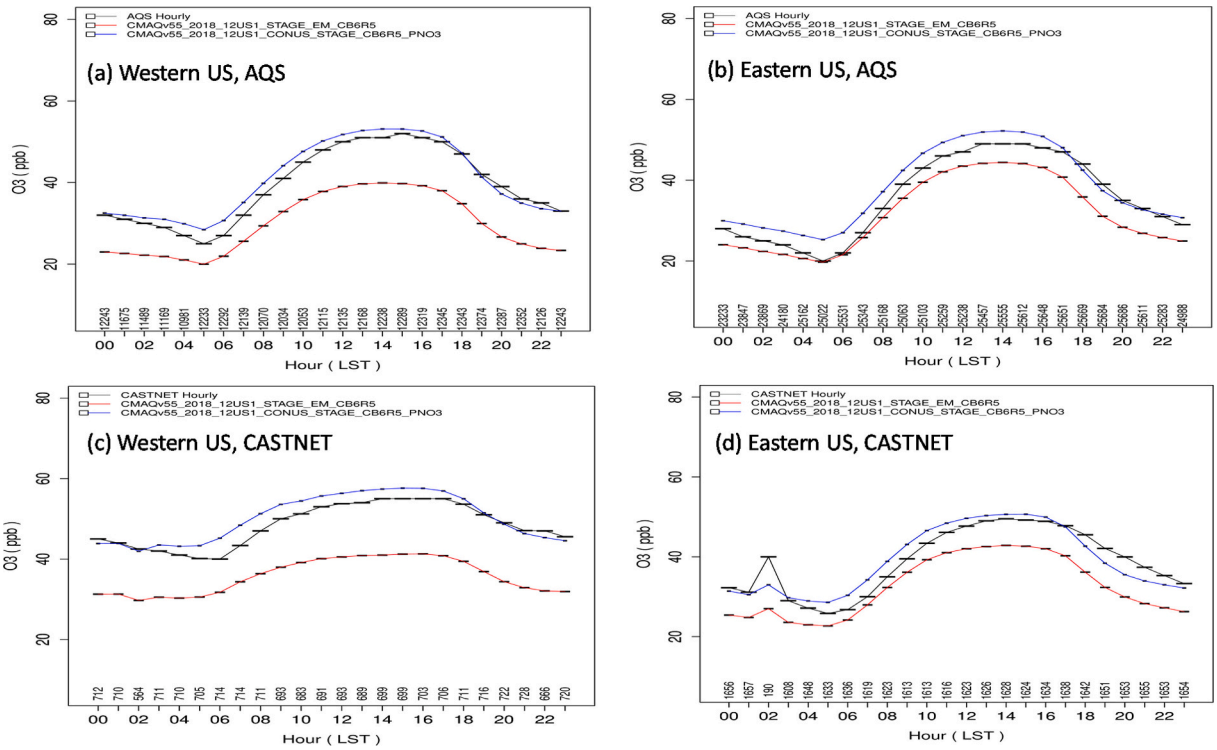

Fig. 7. A comparison of model median diurnal O_3 without (red line, Case A) and with (blue line, Case B) the pNO_3^- photolysis to observed O_3 (black line) in May (a) the western U.S. at AQS sites (b) eastern U.S. at AQS sites (c) Western U.S. at CASTNET sites (d) eastern U.S. at CASTNET sites. The number of observed and model values at each hour is shown above the x-axis. Horizontal black bars in the figure represent median values at each hour.

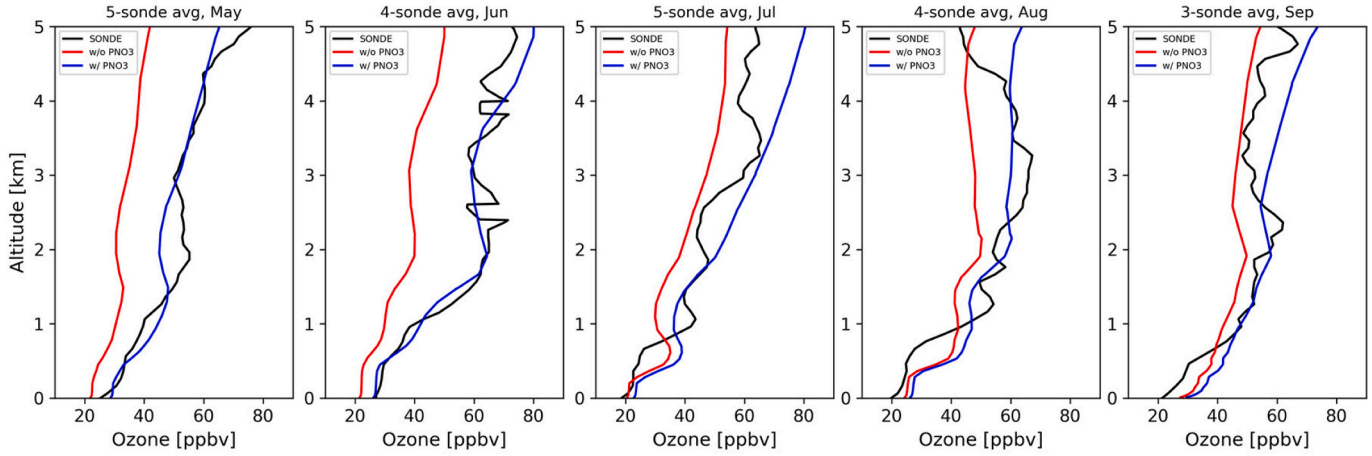

Fig. 8. (a) A comparison of median modeled O_3 without (red line, Case A) and with (blue line, Case B) the pNO_3^- photolysis compared to median ozonesonde data (black line) at Trinidad Head in California for all sonde data in May (left-hand plot), June (second-from left), July (center plot), August (second from right) and September (right-hand plot).

results with pNO_3 photolysis agree better with observed data at lower altitudes and model results without pNO_3 photolysis agree better with observed data at higher altitudes. In September, model results without pNO_3 photolysis agree better with observed data at all altitudes except at very low altitude where the model without pNO_3 photolysis produces lower and the model with pNO_3 photolysis produces higher values than observed data. In Huntsville, the model produces mixed results. Model results without pNO_3 photolysis agree better with observed data at lower altitudes while results with pNO_3 photolysis agree better with observed data at higher altitude in some months.

4. Sensitivity study

We calculate impacts of pNO_3 photolysis occurring over the model domain on May MDA8 O_3 by subtracting model results of the first simulation (Case A, which did not include any pNO_3 photolysis) from the model results with the sensitivity simulation (Case C, which includes pNO_3 photolysis). We calculate the impacts of integrating the effect of pNO_3 photolysis into boundary condition by subtracting model results of the sensitivity simulation (Case C) from the model results with the second simulation (Case B, which includes pNO_3 photolysis and the effect of pNO_3 photolysis was integrated into boundary condition). The impacts of the pNO_3 photolysis without integrating the effect of pNO_3

photolysis in boundary conditions on MDA8 O_3 reach up to 8 ppbv (Fig. 9(a)) while the impacts of integrating the effect of pNO_3 photolysis into boundary condition are higher and reach up to 16 ppbv (Fig. 9(b)). Higher impacts occur over the western U.S. than the eastern U.S. in both cases. In essence, Fig. 9(a) shows the modeled impact of pNO_3 photolysis on MDA8 O_3 within the model domain while Fig. 9(b) shows the impact from long-range transport outside the 12-km modeling domain. The mean MDA8 O_3 enhancement over the U.S. due to both effects is 11.0 ppbv, due to the boundary condition effect of pNO_3 photolysis is 7.5 ppbv, and due to the photolysis of pNO_3 from within the limited area domain is 3.5 ppbv. Thus, the mean MDA8 O_3 enhancement over the U.S. due to the boundary condition effect of pNO_3 photolysis is >2 times greater than the mean enhancement due to the photolysis of pNO_3 from within the limited area domain. Therefore, modeling with pNO_3 photolysis using the effect of pNO_3 photolysis in boundary conditions has a much larger impact on model O_3 over the U.S. than the model without using the effect of pNO_3 photolysis in boundary conditions. To calculate fractional impact of the pNO_3 photolysis within the modeling domain on MDA8 O_3, we divide the results in Fig. 9(a) by the sum of results in Figs. 9(a) and 9(b). Similarly, to calculate fractional impact of integrating the effect of pNO_3 photolysis into boundary condition on MDA8 O_3, we divide the results in Fig. 9(b) by the sum of results shown in Figs. 9(a) and 9(b). Fractional impacts of the pNO_3 photolysis and integrating the effect of pNO_3 photolysis into boundary condition on MDA8 O_3 are shown in Fig. 9(c) and 9(d), respectively which show that 50–90 % of the O_3 impacts from pNO_3 photolysis are a result of chemistry occuring outside of the modeling domain. The fraction of O_3 impacts resulting from chemistry within the domain is largest in the southeastern U.S. (40–50 %) and smallest along the northern border of the U.S. (10–20 %). While the fraction of O_3 impacts resulting from pNO_3 photolysis within the domain is the largest in the southeastern U.S. (Fig. 9(c)), it represents a smaller portion of the combined impact as most of the contribution comes from integrating the effect of pNO_3 photolysis into boundary condition (Fig. 9(d)). The combined impact is still largest in the western U.S. [the sum of Figs. 9(a) and 9(b)].

This analysis suggests that long-range transport from remote atmosphere over seawater (outside the 12-km modeling domain) increases O_3 over the U.S. The higher pNO_3 photolysis frequency over remote seawater releases NO_2 and HONO in NO_x limited areas where it can effectively enhance O_3, and this increased O_3 can then be transported into the U.S. pNO_3 photolysis also decreases pNO_3 concentrations over seawater. However, pNO_3 concentrations over seawater are much smaller than those over land. Thus, the transport of lower pNO_3 concentrations from the remote atmosphere over seawater to the U.S. only affects its concentrations by small margins. In addition, the production of pNO_3 via atmospheric reactions in polluted atmosphere over land is higher than over remote areas of seawater. While pNO_3 photolysis also increases HONO and NO_2 over remote areas of seawater, their impacts over land are relatively small since HONO and NO_2 mixing ratios over land are generally much higher than those over remote areas of seawater and additional sources of HONO and NO_2 contribute to the higher mixing ratios over land. Thus, pNO_3 photolysis has a relatively larger impact on O_3 over the U.S. than on pNO_3, HONO, and NO_2. This sensitivity study highlights the importance of integrating the effect of pNO_3 photolysis into boundary conditions for modeling over the U.S.

5. Summary and future direction

Here, we examine the impacts of pNO_3 photolysis over seawater on air quality over the U.S. by using CMAQv5.5 with 12-km horizontal grid resolution. The model simulation with pNO_3 photolysis reduces the pNO_3 concentrations over seawater without affecting the model skill in reproducing the observed data in the U.S. Including pNO_3 photolysis in the model chemistry increases NO_2 mixing ratios over seawater without affecting the comparison of model predictions with surface layer observed data in the U.S. but improves the comparison with satellite

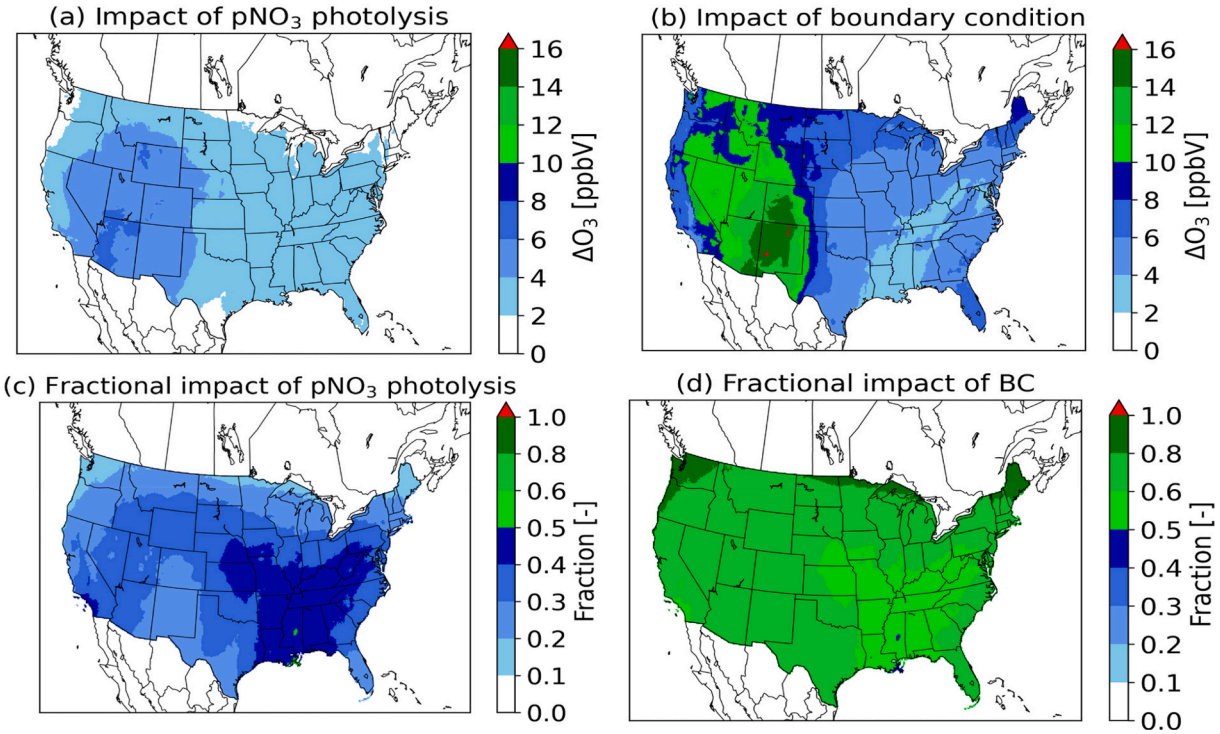

Fig. 9. Sensitivity analysis: (a) Absolute impact of pNO_3^- photolysis on mean MDA8 O_3 in May (boundary condition did not include the effects of pNO_3^- photolysis) (Case C - Case A) (b) absolute impact of integrating the impact of pNO_3^- photolysis into boundary condition on mean MDA8 O_3 in May (the model did not include the pNO_3^- photolysis) (Case B - Case C) (c) fractional impact of pNO_3^- photolysis on mean MDA8 O_3 in May (boundary condition did not include the effects of pNO_3^- photolysis) (d) fractional impact of integrating the impact of pNO_3^- photolysis into boundary condition on mean MDA8 O_3 in May (the model did not include the pNO_3^- photolysis).

retrievals due to increases in upper layer NO_2 mixing ratios. pNO_3 photolysis also increases HONO mixing ratios over seawater but has only small impacts on surface layer HONO over land. Finally, the model predicts that pNO_3 photolysis substantially increases surface layer O_3, improves the model underestimation of springtime O_3 in the U.S., improves the underestimation of model O_3 in the western U.S. in summer and fall, and slightly increases the overestimation in the eastern U.S. Including pNO_3 photolysis in the model chemistry deteriorates the comparison with observed O_3 at lower end of observed data, improves the underestimation of O_3 at higher end of observed data, and improves the model diurnal patterns compared to observed data in the western U.S. in May and July and in the eastern U.S. in May. Model sensitivity results suggest that boundary condition effects account for majority of the impact of pNO_3 photolysis on O_3 in the U.S. Here, we use a simple parameterization for calculating pNO_3 photolysis frequency. However, many factors including pH, relative humidity, temperature, ice and snow, halides, solvent cages, coexisting species, cations, organics, and mineral dust (Gen et al., 2022; Cao et al., 2023) can affect pNO_3 photolysis frequency. Additional field and experimental studies are needed to better characterize the effects of these parameters on pNO_3 photolysis frequency which can then be incorporated into air quality models.

CRediT authorship contribution statement

Golam Sarwar: Writing – review & editing, Writing – original draft, Visualization, Validation, Methodology, Investigation, Formal analysis, Data curation, Conceptualization. **Fahim Sidi:** Writing – review & editing, Software, Methodology, Data curation. **Heather Simon:** Writing – review & editing, Writing – original draft, Investigation, Conceptualization. **Barron H. Henderson:** Writing – review & editing, Writing – original draft, Validation. **Jeff Willison:** Software, Data curation. **Rob Gilliam:** Writing – original draft, Methodology. **Christian Hogrefe:** Writing – review & editing, Software, Methodology. **Kristen Foley:** Writing – review & editing, Software, Methodology. **Rohit Mathur:** Writing – review & editing, Investigation. **Wyat Appel:** Software.

Disclaimer

The views expressed in this paper are those of the authors and do not necessarily represent the views or policies of the U.S. EPA. Mention of trade names or commercial products does not constitute endorsement or recommendation for use.

Declaration of competing interest

The authors declare that they have no known competing financial interests or personal relationships that could have appeared to influence the work reported in this paper.

Appendix A. Supplementary data

Supplementary data to this article can be found online at https://doi.org/10.1016/j.scitotenv.2025.178968.

Data availability

CMAQ source code is publicly available from the following website: https://github.com/USEPA/CMAQ.

References

Alapaty, K., Herwehe, J.A., Otte, T.L., Nolte, C.G., Bullock, O.R., Mallard, M.S., Kain, J.S., Dudhia, J., 2012. Introducing subgrid-scale cloud feedbacks to radiation for regional meteorological and climate modeling. Geophys. Res. Lett. 39, L24808. https://doi.org/10.1029/2012gl054031.

Appel, K.W., Napelenok, S.L., Foley, K.M., Pye, H.O.T., Hogrefe, C., Luecken, D.J., Bash, J.O., Roselle, S.J., Pleim, J.E., Foroutan, H., Hutzell, W.T., Pouliot, G.A., Sarwar, G., Fahey, K.M., Gantt, B., Gilliam, R.C., Heath, N.K., Kang, D., Mathur, R., Schwede, D.B., Spero, T.L., Wong, D.C., Young, J.O., 2017. Description and evaluation of the community multiscale air quality (CMAQ) modeling system version 5.1. Geosci. Model Dev. 10, 1703–1732. https://doi.org/10.5194/gmd-10-1703-2017.

Appel, K.W., Bash, J.O., Fahey, K.M., Foley, K.M., Gilliam, R.C., Hogrefe, C., Hutzell, W. T., Kang, D., Mathur, R., Murphy, B.N., Napelenok, S.L., Nolte, C.G., Pleim, J.E., Pouliot, G.A., Pye, H.O.T., Ran, L., Roselle, S.J., Sarwar, G., Schwede, D.B., Sidi, F.I., Spero, T.L., Wong, D.C., 2021. The Community Multiscale Air Quality (CMAQ) model versions 5.3 and 5.3.1: system updates and evaluation. Geosci. Model Dev. 14, 2867–2897. https://doi.org/10.5194/gmd-14-2867-2021.

Bash, J.O., Baker, K.R., Beaver, M., 2016. R.: evaluation of improved land use and canopy representation in BEIS v3.61 with biogenic VOC measurements in California. Geosci. Model Dev. 9, 2191–2207. https://doi.org/10.5194/gmd-9-2191-2016.

Beidler, J., Pouliot, G., Foley, K., 2024. 2024: 2004–2017 geospatial dataset of wild and prescribed fire activity over the conterminous United States. Data Brief 56, 110856.

Cao, Y., Ma, Q., Chu, B., He, H., 2023. 2023: homogeneous and heterogeneous photolysis of nitrate in the atmosphere: state of the science, current research needs, and future prospects. Front. Environ. Sci. Eng. 17 (4), 48.

Dang, R., Jacob, D.J., Shah, V., Eastham, S.D., Fritz, T.M., Mickley, L.J., Liu, T., Wang, Y., Wang, J., 2023. Background nitrogen dioxide (NO_2) over the United States and its implications for satellite observations and trends: effects of nitrate photolysis, aircraft, and open fires. Atmos. Chem. Phys. 23, 6271–6284. https://doi.org/10.5194/acp-23-6271-2023.

Dennis, R., Fox, T., Fuentes, M., Gilliland, A., Hanna, S., Hogrefe, C., Irwin, J., Venkatram, A., 2010. A framework for evaluating regional-scale numerical photochemical modeling systems. *Environ. Fluid Mechanics 10* (4), 471–489.

Foley, K.M., Pouliot, G.A., Eyth, A., Aldridge, M.F., Allen, C., Appel, K.W., Bash, J.O., Beardsley, M., Beidler, J., Choi, D., Farkas, C., Gilliam, R.C., Godfrey, J., Henderson, B.H., Hogrefe, C., Koplitz, S.N., Mason, R., Mathur, R., Misenis, C., Possiel, N., Pye, H.O.T., Reynolds, L., Roark, M., Roberts, S., Schwede, D.B., Seltzer, K.M., Sonntag, D., Talgo, K., Toro, C., Vukovich, J., Xing, J., Adams, E., 2023. 2002-2017 anthropogenic emissions data for air quality modeling over the United States. Data Brief 47, 109022. https://doi.org/10.1016/j.dib.2023.109022.

Gantt, B.; Kelly, J. T.; and Bash, J. O., 2015. Updating sea spray aerosol emissions in the Community Multiscale Air Quality (CMAQ) model version 5.0.2. Geosci. Model Dev., 8, 3733–3746, doi:https://doi.org/10.5194/gmd-8-3733-2015, 2015.

Gaudel, A., Cooper, O.R., Ancellet, G., Barret, B., Boynard, A., Burrows, J.P., Clerbaux, C., Coheur, P.-F., Cuesta, J., Cuevas, E., Doniki, S., Dufour, G., Ebojie, F., Foret, G., Garcia, O., Granados-Muñoz, M.J., Hannigan, J.W., Hase, F., Hassler, B., Huang, G., Hurtmans, D., Jaffe, D., Jones, N., Kalabokas, P., Kerridge, B., Kulawik, S., Latter, B., Leblanc, T., Le Flochmoën, E., Lin, W., Liu, J., Liu, X., Mahieu, E., McClure-Begley, A., Neu, J.L., Osman, M., Palm, M., Petetin, H., Petropavlovskikh, I., Querel, R., Rahpoe, N., Rozanov, A., Schultz, M.G., Schwab, J., Siddans, R., Smale, D., Steinbacher, M., Tanimoto, H., Tarasick, D.W., Thouret, V., Thompson, A.M., Trickl, T., Weatherhead, E., Wespes, C., Worden, H.M., Vigouroux, C., Xu, X., Zeng, G., Ziemke, J., 2018. Tropospheric Ozone Assessment Report: Present-Day Distribution and Trends of Tropospheric Ozone Relevant to Climate and Global Atmospheric Chemistry Model Evaluation, vol. 6 39. Science of the Anthropocene, Elementa. https://doi.org/10.1525/elementa.291, 1 January.

Gen, M., Liang, Z., Zhang, R., Mabato, B., R, G.; Chan, C. K., 2022. Particulate nitrate photolysis in the atmosphere. Environmental Science: Atmospheres 2 (2), 111–127.

Gilliam, R.C., Herwehe, J.A., Bullock Jr., O.R., Pleim, J.E., Ran, L., Campbell, P.C., Foroutan, H., 2021. Establishing the suitability of the model for prediction across scales for global retrospective air quality modeling. J. Geophys. Res. Atmos. 126, e2020JD033588. https://doi.org/10.1029/2020JD033588.

Herwehe, J.A., Alapaty, K., Spero, T.L., Nolte, C.G., 2014. Increasing the credibility of regional climate simulations by introducing subgrid-scale cloud-radiation interactions. J. Geophys. Res. Atmos. 119, 5317–5330. https://doi.org/10.1002/2014JD021504.

Iacono, M.J., Delamere, J.S., Mlawer, E.J., Shephard, M.W., Clough, S.A., Collins, W.D., 2008. Radiative forcing by long-lived greenhouse gases: calculations with the AER radiative transfer models. J. Geophys. Res. 113, D13103. https://doi.org/10.1029/2008JD009944.

Johnson, Bryan J., Cullis, Patrick D., NOAA ESRL, 2018. Earth system research laboratory ozone water vapor group Ozonesonde measurements, version 1. NOAA National Centers for Environmental Information. https://doi.org/10.7289/V5CC0XZ1 [January 7, 2025]. https://www.ncei.noaa.gov/access/metadata/landing-page/bin/iso?id=gov.noaa.ncdc:C01563.

Kain, J.S., 2004. The Kain-Fritsch convective parameterization: an update. J. Appl. Meteorol. 43, 170–181.

Kang, D., Pickering, K. E., Allen, D. J., Foley, K. M., Wong, D. C., Mathur, R., and Roselle, S. J., 2019: simulating lightning NO production in CMAQv5.2: evolution of scientific updates, Geosci. Model Dev. 2019 12, 3071–3083. doi:https://doi.org/10.5194/gmd-12-3071-2019.

Krotkov, N.A., Lamsal, L.N., Celarier, E.A., Swartz, W.H., Marchenko, S.V., Bucsela, E.J., Chan, K.L., Wenig, M., Zara, M., 2017. The version 3 OMI NO_2 standard product. Atmos. Meas. Tech. 10, 3133–3149. https://doi.org/10.5194/amt-10-3133-2017.

Lefohn, A.S., Malley, C.S., Simon, H., Wells, B., Xu, X., Zhang, L., Wang, T., 2017. Responses of human health and vegetation exposure metrics to changes in ozone concentration distributions in the European Union, United States, and China. Atmos. Environ. 152, 123–145.

Mathur, R., Xing, J., Gilliam, R., Sarwar, G., Hogrefe, C., Pleim, J., Pouliot, G., Roselle, S., Spero, T.L., Wong, D.C., Young, J., 2017. Extending the community multiscale air

quality (CMAQ) modeling system to hemispheric scales: overview of process considerations and initial applications. Atmos. Chem. Phys. 17, 12449–12474. https://doi.org/10.5194/acp-17-12449-2017.

Millero, F.J., 1996. Chemical Oceanography, second ed. CRC Press, Boca Raton, FL.

Morrison, H., Thompson, G., Tatarskii, V., 2009. Impact of cloud microphysics on the development of trailing stratiform precipitation in a simulated squall line: comparison of one- and two-moment schemes. Mon. Weather Rev. 137, 991–1007.

Napelenok, S. L., Kristen M. Foley, Daiwen Kang, Rohit Mathur, Thomas Pierce, S. Trivikrama Rao, 2011: Dynamic evaluation of regional air quality model's response to emission reductions in the presence of uncertain emission inventories, Atmospheric Environment, Volume 45, Issue 24, 2011, Pages 4091-4098, ISSN 1352–2310, doi:https://doi.org/10.1016/j.atmosenv.2011.03.030.

Pleim, J.E., 2006. A simple, efficient solution of flux-profile relationships in the atmospheric surface layer. J. Appl. Meteorol. Climatol. 45, 341–347.

Pleim, J.E., 2007. A combined local and nonlocal closure model for the atmospheric boundary layer. Part I: model description and testing. J. Appl. Meteorol. Climatol. 46, 1383–1395.

Pleim, J.E., Gilliam, R.C., 2009. An indirect data assimilation scheme for deep soil temperature in the Pleim-Xiu land Surface model. J. Appl. Meteor. Climatol. 48, 1362–1376.

Pleim, J.E., Xiu, A., 1995. Development and testing of a surface flux and planetary boundary layer model for application in mesoscale models. J. Appl. Meteorol. Climatol. 34, 16–32.

Reed, et al., 2017. Evidence for renoxification in the tropical marine boundary layer. Atmos. Chem. Phys. 17, 4081–4092.

Romer, P.S., Wooldridge, P.J., Crounse, J.D., Kim, M.J., Wennberg, P.O., Dibb, J.E., Scheuer, E., Blake, D.R., Meinardi, S., Brosius, A.L., Thames, A.B., Miller, D.O., Brune, W.H., Hall, S.R., Ryerson, T.B., Cohen, R.C., 2018. Constraints on aerosol nitrate photolysis as a potential source of HONO and NO_x. Environ. Sci. Technol. 52 (23), 13738–13746. https://doi.org/10.1021/acs.est.8b03861.

Russel, A., and Dennis, R., 2000: NARSTO critical review of photochemical models and modeling, Atmospheric Environment, Volume 34, Issues 12–14, 2000, Pages 2283-2324, ISSN 1352–2310, doi:https://doi.org/10.1016/S1352-2310(99)00468-9.

Sarwar, G., Roselle, S.J., Mathur, R., Appel, W., Dennis, R.L., Vogel, B., 2008. A comparison of CMAQ HONO predictions with observations from the northeast oxidant and particle study. Atmos. Environ. 42, 5760–5770.

Sarwar, G., Henderson, B.H., Hogrefe, C., Mathur, R., Gilliam, R., Callaghan, A., B., Lee, J., Carpenter, L. J., 2024. Examining the impact of the photolysis of aerosol nitrate over northern hemisphere. Sci. Total Environ. 917 (170406), 2024. https://doi.org/10.1016/j.scitotenv.2024.170406.

Shah, V., Jacob, D.J., Dang, R., Lamsal, L.N., Strode, S.A., Steenrod, S.D., Boersma, K.F., Eastham, S.D., Fritz, T.M., Thompson, C., Peischl, J., Bourgeois, I., Pollack, I.B., Nault, B.A., Cohen, R.C., Campuzano-Jost, P., Jimenez, J.L., Andersen, S.T., Carpenter, L.J., Sherwen, T., Evans, M.J., 2023. Nitrogen oxides in the free troposphere: implications for tropospheric oxidants and the interpretation of satellite NO_2 measurements. Atmos. Chem. Phys. 23, 1227–1257. https://doi.org/10.5194/acp-23-1227-2023.

Shi, Q., Tao, Y., Krechmer, J.E., Heald, C.L., Murphy, J.G., Kroll, J.H., Ye, Q., 2021. Laboratory investigation of Renoxification from the photolysis of inorganic particulate nitrate. Environ. Sci. Technol. 55 (2), 854–861. https://doi.org/10.1021/acs.est.0c06049.

Simon, H., Reff, A., Wells, B., Xing, J., Frank, N., 2015. Ozone trends across the United States over a period of decreasing NOx and VOC emissions. Environ. Sci. Technol. 49, 186–195.

Skamarock, W.C., Klemp, J.B., Dudhia, J., Gill, D.O., Liu, Z., Berner, J., Wang, W., Power, J.P., Duda, M.G., Barker, D., Huang, X., 2021. A description of the advanced research WRF. Model Version 4.3 (No. NCAR/TN-556+STR). https://doi.org/10.5065/1dfh-6p97.

Stauffer, D.R., Seaman, N.L., 1990. Use of four-dimensional data assimilation in a limited-area model, part I: experiments with synoptic-scale data. Mon. Weather Rev. 118, 1250–1277.

EPA, U.S., 2019. Meteorological model performance for annual 2016 simulation WRF v3.8. Office of Air Quality Planning and Standards. U.S. Environmental Protection Agency. EPA-454/R-19-010. https://www3.epa.gov/ttn/scram/reports/Met_Model_Performance-2016_WRF.pdf.

US EPA, 2020a: Integrated science assessment for ozone and related photochemical oxidants, Center for Public Health and Environmental Assessment Office of Research and Development U.S. Environmental Protection Agency research Triangle Park, NC, EPA/600/R-20/012.

US EPA, 2020b: Policy assessment for the review of the ozone National Ambient air Quality Standards, U.S. Environmental Protection Agency Office of air quality planning and standards health and environmental impacts division research Triangle Park, NC, EPA-452/R-20-001.

US EPA, 2021. 2017 National Emissions Inventory: January 2021 updated release, technical support document, EPA-454/R-21-001. U.S. Environmental Protection Agency Office of air quality planning and standards air quality assessment division emissions inventory and analysis group research Triangle Park, NC, EPA-454/R-21-001.Available at: https://www.epa.gov/sites/default/files/2019-12/documents/2016fe_hemispheric_tsd.pdf.

Wells, B., et al., 2021: Improved estimation of trends in U.S. ozone concentrations adjusted for interannual variability in meteorological conditions. Atmospheric environment, volume 248, 1 march 2021, 118234.

Yarwood, G., Shi, Y., Beardsley, R., 2020: Impact of CB6r5 Mechanism Changes on Air Pollutant Modeling in Texas, Final Report to Texas Commission on Environmental Quality, Work Order No. 582–20–11221-014, July, 2020.

Ye, C., Zhou, X., Pu, D., et al., 2016. Rapid cycling of reactive nitrogen in the marine boundary layer. Nature 532, 489–491. https://doi.org/10.1038/nature17195.

Ye, C., Zhang, Ni, Gao, H., Zhou, X., 2017. Photolysis of particulate nitrate as a source of HONO and NO_x. Environ. Sci. Technol. 51 (12), 6849–6856. https://doi.org/10.1021/acs.est.7b00387.

Zhu, Y., Wang, Y., Zhou, X., Elshorbany, Y.F., Ye, C., Hayden, M., Peters, A.J., 2022. An investigation into the chemistry of HONO in the marine boundary layer at Tudor Hill marine atmospheric Observatory in Bermuda. Atmos. Chem. Phys. 22, 6327–6346. https://doi.org/10.5194/acp-22-6327-2022.